The Avrami Index and the Fractal Dimension in Vegetable Oil Crystallization

Jorge F. Toro-Vazquez[a,*], Elena Dibildox-Alvarado[a], Miriam Charó-Alonso[a], Veronica Herrera-Coronado[b], and Carlos A. Gómez-Aldapa[a]

[a]Facultad de Ciencias Químicas, Universidad Autónoma de San Luis Potosí, Zona Universitaria, San Luis Potosí, 78210 México, and [b]PROPAC Facultad de Química-DIPA, Universidad Autónoma de Querétaro, Cerro de las Campanas S.N., Querétaro, México

ABSTRACT: The behavior of the Avrami plot during TAG crystallization was studied by DSC and rheological measurements in oil blends of palm stearin (26 and 80%) in sesame oil, using different crystallization temperatures (T_{Cr}°) attained under several cooling rate conditions (1, 10, and 30°C/min). In the same way, the relationship between the growth mechanisms of TAG, measured by the Avrami index (*n*), and the mass fractal dimension (*D*) of the crystal network was investigated. This last parameter was measured as TAG crystallized in the oil blend under isothermal conditions. Results showed that TAG crystallization in a vegetable oil involves the process of TAG lamellar development, nucleation, and crystal growth. Each event occurred at a different rate and extent as affected by cooling rate and T_{Cr}°, and as a function of crystallization time under isothermal conditions at a given cooling rate. Within this framework, we proposed that *n* calculated from the second region of the Avrami plot is a parameter mainly associated with crystal growth, whereas *n* from the first region is associated more with nucleation. On the other hand, changes in *D* values followed the different polymorphic states developed by TAG as a function of T_{Cr}°. Additionally, it was shown that, independent of the concentration of palm stearin in the oil blend, at cooling rates of 1 and 10°C/min the increase in *n* from ≈3 to ≈4 produced a curvilinear increase in *D* from ≈1.75 to ≈3.0. The growth mechanism of the TAG crystals (i.e., *n*), also affected the magnitude of *D*. However, different behavior was observed in the *n*–*D* relationship when $n < 2.7$ and at 30°C/min.

Paper no. J10192 in *JAOCS 79*, 855–866 (September 2002).

KEY WORDS: Avrami, cooling rate, fractal, fractal dimension, oil crystallization, palm oil, sesame oil.

The development of TAG crystals in vegetable oils is a complex process. Thus, before TAG crystallize, the system must have the thermodynamic drive to develop a solid from a liquid phase, i.e., supercooling. Such a condition is attained by a decrease in temperature below the point where the smallest aggregates of molecules in the solid phase (i.e., unstable crystal nuclei) are in equilibrium with the molecules in the liquid phase (i.e., TAG in lamellar "liquid organization" in the vegetable oil). This temperature is the equilibrium melting temperature T_M°. Supercooling is needed to structure the molecules into a "liquid structure." Thus, TAG molecules develop a local order until a critical size of TAG monomer aggregates is achieved and thermodynamically stable solid nuclei are formed (1,2). Once nucleation occurs, additional events (i.e., crystal growth, crystal perfection, and polymorphism) take place in parallel at different rates. During this process, TAG develop, in the oil continuum, a 3-D network with a fractal organization (3,4). The mechanical properties of the crystallized system depend on the fractal geometry of the network and on the forces that keep the crystal aggregated. In fact, it has been shown that the fractal dimension that characterizes the crystal network of TAG (*D*) has a mathematical relationship with textural parameters of crystallized systems such as hardness (4).

The process of TAG crystallization in vegetable oils might be studied through several models (2). However, the most extensively used is the Avrami model. This model (Eq. 1) has been used primarily in the determination of *n*, the exponent in the Avrami equation, the value of which is associated with the mechanisms of crystal growth. Thus, in homogeneous nucleation a crystallization process with $n = 4$ follows a 3-D crystal growth mechanism, a value of $n = 3$ a 2-D mechanism, and $n = 2$, 1-D crystal growth. Noninteger values of *n* are associated with heterogeneous and secondary nucleation. Additionally, in the Avrami equation (Eq. 1), *z* is a composite rate constant involving nucleation and crystal growth rate, and *F* denotes reduced crystallinity since it associates the crystallinity of the system at a given time (*t*) with the total crystallinity achieved under the experimental conditions. The *F* value is calculated with a property proportional to the change in solid phase or crystallinity developed in the system as a function of time (2).

$$1 - F = \exp(-zt^n) \quad [1]$$

$$\ln[-\ln(1 - F)] = \ln(z) + n[\ln(t)] \quad [2]$$

The values of *n* and *z* are calculated from the linear form of the Avrami equation (Eq. 2) as the slope and intercept at $\ln(t) = 0$, respectively. This procedure assumes that a single slope, associated with the value of *n*, is obtained from a plot of $\ln[-\ln(1 - F)]$ vs. $\ln(t)$. However, the application of Equation 2 to crystallization data from vegetable oils has given

*To whom correspondence should be addressed at Facultad de Ciencias Químicas, Universidad Autónoma de San Luis Potosí, Av. Dr. Manuel Nava 6, Zona Universitaria, San Luis Potosí, 78210, México. E-mail: toro@uaslp.mx

Copyright © 2002 by AOCS Press

inconsistent results, and most of the time two regions with different slopes have been obtained (3).

Within this framework our laboratory has been engaged in crystallization experiments using blends of palm stearin (PS) in sesame oil (1,3,5). This research was done to study, in a complex model system, the crystallization of saturated TAG in a mixture with highly unsaturated TAG. PS is a mixture of highly saturated TAG obtained through fractional crystallization from refined, bleached, and deodorized palm oil. Tripalmitin is the TAG with the highest melting temperature in both palm oil (5–10% w/w) and PS (12–56% w/w). Consequently, tripalmitin determines to a great extent the crystallization kinetics and polymorphic transformations of PS and PS/sesame oil blends (5,6). In contrast, sesame oil is a highly unsaturated vegetable oil, of which the main components are oleic (38–43%) and linoleic acids (40–44%) (1,5).

The objective of this investigation was to evaluate, through DSC and rheological measurements, the process of TAG crystallization in PS/sesame oil blends at supercooling conditions achieved at different cooling rates. A likely explanation regarding the different slopes obtained with the use of the Avrami model in vegetable oil crystallization was developed. Additionally, we studied the possible relationships between the growth mechanisms followed by TAG and the 3-D crystal network developed by the oil blends during crystallization. This was done by considering that D is a fundamental constant of the crystal network structure, whereas n is associated with the crystal growth mechanism.

MATERIALS AND METHODS

Oil sample preparation. Whole-seed refined sesame oil was obtained from a local industry (DIPASA de Mexico, Celaya, Gto., Mexico). Refined, bleached, and deodorized PS was provided by the Palm Oil Research Institute of Malaysia (Kuala Lumpur, Malaysia). The same batches of sesame oil and PS were used in all experiments. Blends of PS in sesame oil (26 and 80%, wt/vol) were prepared by adding the oil (25°C) to a given weight of PS (60°C) and mixing the system at 80°C for 30 min with a magnetic stirrer.

DSC studies. Crystallization studies were done in a model DSC-7 PerkinElmer differential scanning calorimeter (PerkinElmer, Norwalk, CT) equipped with a dry box. Temperature was calibrated with indium (onset temperature for melting = 156.6°C) and *n*-hexatriacontane (onset temperature for melting = 76.1°C), and a baseline for volatile substances was developed with empty aluminum pans. Heat involved in phase changes (i.e., melting/crystallization) was calibrated with indium alone (ΔH for melting = 28.45 J/g).

The sample of oil (≈12 mg) was sealed in a pan and held at 80°C for 30 min to melt all crystals (e.g., erase crystallization memory). After this time, the system was cooled at a given rate until the crystallization temperature was reached. The cooling rates investigated were 1, 10, and 30°C/min. After completion of the crystallization exotherm (i.e., heat capacity returned to the baseline), the system was left at the isothermal temperature for an additional 35 min. Afterward, the melting thermogram was obtained by heating the system at a rate of 5.0°C/min. The induction time of crystallization by DSC, τ_{iDSC}, was calculated according to Toro-Vazquez *et al.* (7) using the first derivative of the crystallization exotherm calculated with the DSC software library (Pyris^{TM}), i.e., τ_{iDSC} is the time at which the first derivative of the heat capacity of the sample initially departed from the baseline (Fig. 1). In the same way, F values from the crystallization exotherm were calculated as described previously (1) using the DSC software library. In short, $F = \Delta H_t/\Delta H_{tot}$, where ΔH_t is the area under the DSC exothermal crystallization curve from $t = \tau_{iDSC}$ to $t = t$, and ΔH_{tot} is the total area under the crystallization curve. For each cooling rate and isothermal crystallization temperature, F, as a function of the crystallization time, was fitted to the linear format of the Avrami equation (Eq. 2). The Avrami index (n) was calculated from the slope.

For the 26% PS/sesame oil blend, the crystallization temperatures were between 24.5° and 27.5°C, whereas for the 80% oil blend, the temperatures were between 33 and 36°C. At least two determinations were done in each case.

Rheological measurements. By using the same crystallization conditions as for DSC measurements, the storage modulus (G'), loss modulus (G''), and phases shift angles (δ) of the oil blends were measured during crystallization. A dynamic mechanical spectrometer (Parr Physica UDS 200; Stuttgart, Germany) with parallel plates geometry (50 mm in diameter and a gap of 1 mm) equipped with a Peltier temperature control was used for the measurements. Temperature and cooling rates were programmed using the software on the equipment (Universal Software US 200; Parr Physica). The oil blend (80°C) was applied on the base of the plate (40°C) avoiding the formation of air bubbles, and the superior plate was positioned on the sample surface using the auto-gap function available in the software library (Universal Software US 200; Parr Physica). The sample was heated (80°C for 30 min) and then cooled at either 1, 10, or 30°C/min until the crystalliza-

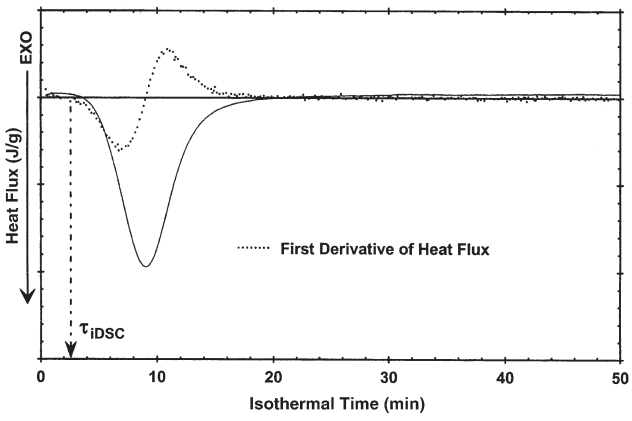

FIG. 1. Thermogram for the 80% palm stearin/sesame oil blend crystallized at 33°C and a cooling rate of 10°C/min. The dotted line shows the first derivative of the heat flux. The induction time for crystallization determined by this methodology is also shown (τ_{iDSC}).

tion temperature was reached. The 30°C/min cooling rate was within the limit of the cooling rate capacity of the equipment, and at the lowest crystallization temperatures investigated, variable cooling rates were obtained. Therefore, rheological data with the 26% oil blend were not reliable and were not included in the analysis. The linear viscoelastic region (LVR) for the oil blends was determined at each crystallization temperature and for different stages of crystallization (i.e., different times of crystallization) using a constant angular frequency of 5 s^{-1} for the 26% blend and 10 s^{-1} for the 80% blend). With this information, oscillatory stress programs were established with the rheometer software to apply a strain to the sample, varying according to the LVR for the different crystallization stages. The strain conditions used to achieve rheological measurements within the LVR varied (strain 0.01–40%; 0.015–20 mrad) as a function of the blend analyzed, crystallization temperature evaluated, and the stage of crystallization. Rheograms were obtained by plotting G', G'', and δ vs. time.

Measurement of the fractal dimension. Measurement of the mass fractal dimension (D) of the TAG crystal network was based on the weak-link regime for colloidal dispersions (i.e., systems with a high volume fraction of solids) (4). In these systems G' increases as a function of the volume fraction of solid fat (ϕ) following Equations 3 and 4:

$$G' = \gamma \phi^m \quad [3]$$

$$\ln(G') = \ln(\gamma) + m[\ln(\phi)] \quad [4]$$

$$m = 1/(3 - D) \quad [5]$$

where m depends on the mass fractal dimension (Eq. 5), and γ is a constant independent of ϕ but dependent on the size of the primary particles and on the interactions between them (4) (i.e., on the polymorphic nature of the fat).

Then, with the assumption that $F \approx \phi$, plots of $\ln(G')$ vs. $\ln(F)$ evaluated the development of the fractal organization during TAG crystallization (Eq. 6). This may be done as long as both parameters are measured at identical crystallization times. Thus, D was calculated from the linear slope, m (Eq. 5), of the $\ln(G')$ vs. $\ln(F)$ curves.

$$\ln(G') = \ln(\gamma) + m[\ln(F)] \quad [6]$$

Statistical analysis. The effect of cooling rate and crystallization temperature on n and D for a particular oil blend was evaluated using a factorial design with two replicates per treatment. Comparisons among treatments were done with orthogonal contrasts using Statistica (v. 5.1, StatSoft, Inc. Tulsa, OK).

RESULTS AND DISCUSSION

The Avrami model at the different cooling rates. Some crystallization and melting thermograms for the 26 and 80% PS/sesame oil blends are shown in Figure 2. Different structures of the crystal polymorphs have been obtained from palm oil and PS as a function of crystallization temperature (6) and

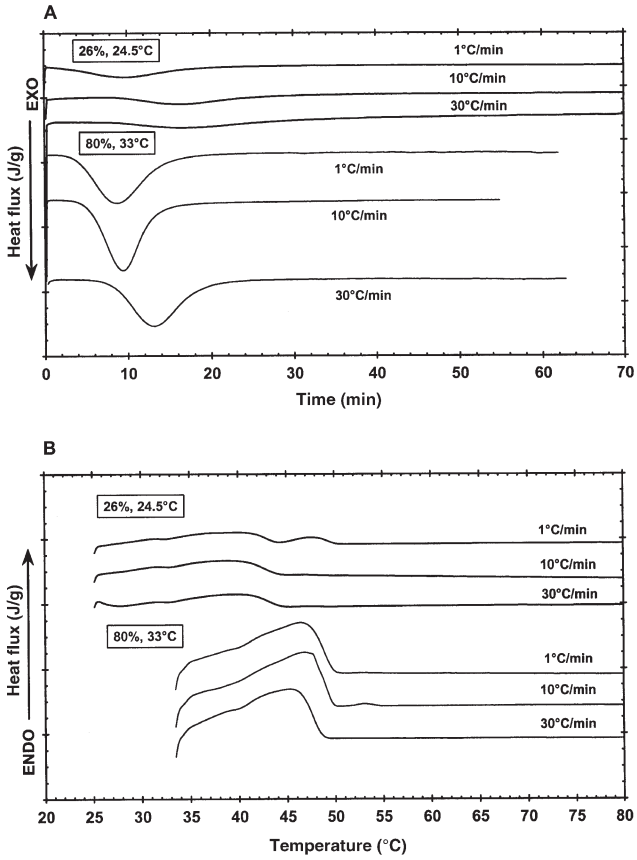

FIG. 2. Crystallization (A) and melting (B) thermograms for the 26 and 80% palm stearin/sesame oil blends. The cooling rate used to achieve isothermal crystallization in each case is indicated. Heating rate during melting was 5°C/min for all samples.

the concentration of PS in an oil blend (1). Such structures have been established through X-ray techniques and analysis of crystallization kinetics (as discussed later in the manuscript). The crystallization exotherm (Fig. 2A) was used to calculate the F values as a function of the isothermal time. The resulting plots of the linear form of the Avrami equation, $\ln[-\ln(1 - F)]$ vs. $\ln(t)$, were intended to provide a single slope associated with the value of n. However, Avrami plots for the oil blends resulted in two regions with different slopes (Fig. 3). The time and F values limiting these two regions varied as a function of the concentration of PS and the crystallization temperature (Fig. 3). Similar behavior in Avrami plots has been observed for Ivory Coast cocoa butter and for an anhydrous milk fat fraction (Ref. 8, Fig. 3). However, in those cases a single slope was fitted to the Avrami data.

In an attempt to understand the crystallization events involved in the two regions, the δ profile during crystallization of the oil blends was superimposed on the corresponding Avrami plots (Figs. 4 and 5). Our group previously used the same approach (7) to study TAG nucleation and crystal growth when the induction time of crystallization (τ_i) was measured by DSC (τ_{iDSC}) and scanning diffusive light scattering (τ_{iSDLS}). Our study (7) showed that the τ_{iDSC} measurement

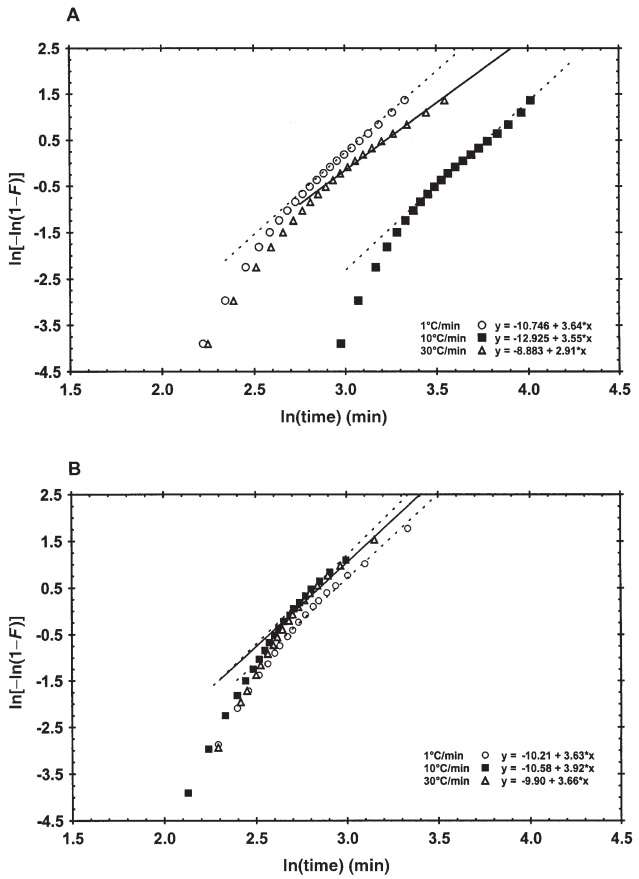

FIG. 3. Avrami plots for the 26 and 80% palm stearin/sesame oil blends at 27.5 (A) and 35°C (B), respectively. The linear regressions for the second region of the plot are indicated for the different cooling rates used.

is associated primarily with crystal growth, whereas τ_{iSDLS} provides a better evaluation of the actual nucleation process. An example of a similar superimposition of the δ profile on the DSC thermogram is shown in Figure 6. However, when using different equipment to evaluate crystallization kinetics, comparisons between results must be done with caution. Differences in weight or volume of samples used, equipment design and its impact on the thermodynamics of the system, and heat and mass transfer conditions existing in each measurement device affect crystallization to a different extent. Such factors must be keep in mind when comparing crystallization data obtained with different equipment, such as when superimposing the DSC and rheological data shown in Figures 4 to 6.

Before discussing the results shown in Figures 4 and 5, some rheological concepts useful in the evaluation of TAG crystallization must be described. In a purely viscous system (i.e., vegetable oil), δ is 90° and subsequently $G' = 0$ and $G'' = G^*$, where G^* is the complex modulus. Once TAG nucleation occurs, a decrease in δ should accompany the phase change from liquid (i.e., vegetable oil blend) to solid with a corresponding increase in the storage modulus (i.e., $G' > 0$). Eventually, if the system becomes fully crystallized (i.e., purely elastic), $\delta = 0°$ and subsequently $G' = G^*$ and $G'' = 0$. Thus, the results in Figures 4 and 5 show that at the lower cooling rate investigated (i.e., 1°C/min), a solid-like behavior was already in effect ($\delta << 90°$) in the oil blends from the very beginning of measurement (i.e., isothermal crystallization) (Figs. 4A and 4C). An exception to this was the crystallization temperature of 36°C, which provided the lowest degree of supercooling of the temperatures investigated (Fig. 5A). In contrast, when cooling rates of 10 or 30°C/min were used, the evolution from liquid toward solid (from $\delta \approx 90°$ to $\delta << 90°$) was observed during isothermal crystallization (Figs. 4B, 5B, and 5C). These results showed that at the low cooling rate used (1°C/min), TAG molecules had enough time to achieve local order in the liquid state, possibly in the form of lamellar structures. Under such conditions, TAG might even have nucleated while temperature decreased toward isothermal crystallization conditions. This last point is in agreement with previous results that compared G' and G'' profiles with τ_i measurements obtained by SDLS (7). In contrast, at 10°C/min (Figs. 4B and 5B), and particularly at 30°C/min (Fig. 5C), TAG molecules had less time to achieve local order in the liquid state while temperatures decreased. A similar phenomenon occurred at 1°C/min at the highest crystallization temperature investigated (i.e., the lowest degree of supercooling) (Fig. 5A). Under such crystallizing conditions, the local order of TAG molecules must be attained mainly during the isothermal period. In these cases, the nucleation was observed as a sharp decrease in δ from $\delta \approx 90°$ to $\delta << 90°$, i.e., the evolution from liquid toward solid-like behavior. A similar sharp decrease in δ was observed right after τ_{iSDLS}, whereas τ_i by DSC (τ_{iDSC}) occurred at later crystallization stages (7). SDLS is quite a sensitive technique and detects the development of a solid phase during crystallization (i.e., nucleation) very well in advance of DSC (7). Consequently, the rapid decline in δ from its original value ($\delta \approx 90°$), as observed in Figures 4 to 6, is associated with TAG nucleation (7).

On the other hand, after the sharp decrease in δ, a peak was observed in all δ rheograms (Figs. 5 and 6). Previous research had shown that, whereas a sharp decrease in δ is associated with the process of nucleation, the δ peak corresponds closely to the TAG crystallization exotherm obtained by DSC (7). The same correspondence between the δ peak and the crystallization exotherm was observed in the present investigation (Fig. 6). In fact, τ_{iDSC} had a close correspondence with the beginning of the δ peak (Fig. 6). Crystal growth is associated with heat released from the binding of TAG molecules on the growing crystal mass. Consequently, the peak observed in the δ rheogram was mainly involved in the measurement of the crystal growth process, whereas the sharp decrease in δ was associated with the process of nucleation (7). Based on the behavior of the δ profile, we might develop a scheme showing the relative contributions of the processes of nucleation and crystal growth during isothermal crystallization. This approach is discussed later on in the manuscript.

As discussed above, it was apparent that TAG crystallization from the melt (i.e., of vegetable oils) involved development

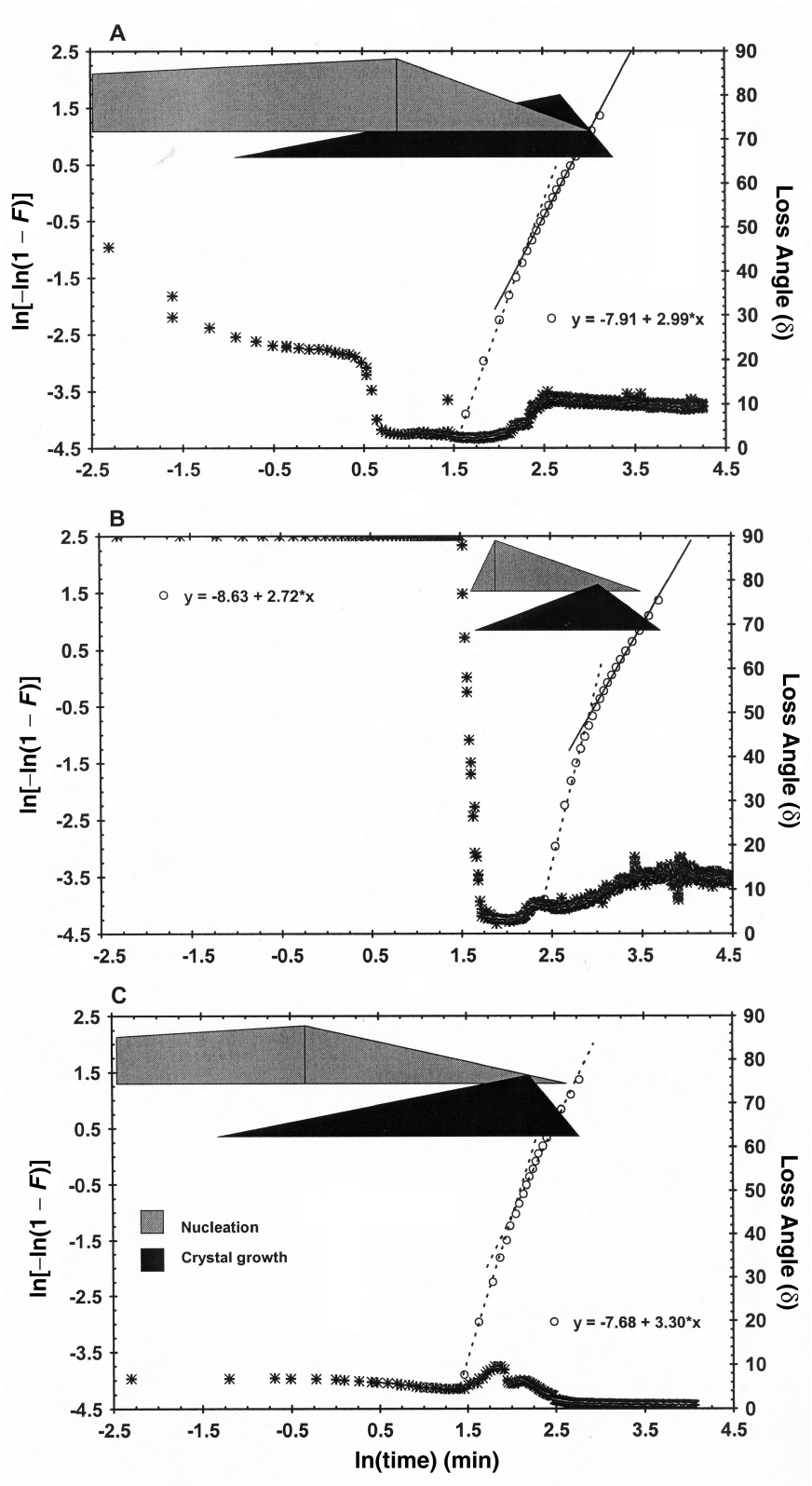

FIG. 4. Avrami plots for the 26% palm stearin/sesame oil blend at 25.5°C at a cooling rate of 1°C/min (A) and 10°C/min (B); and for the 80% oil blend at 33°C at a cooling rate of 1°C/min (C). The corresponding rheogram for the loss angle (δ) is superimposed for comparison purposes. Shadow regions indicate the relative contributions of nucleation and crystal growth to the crystallization process. The rest of the legend is as in Figure 3.

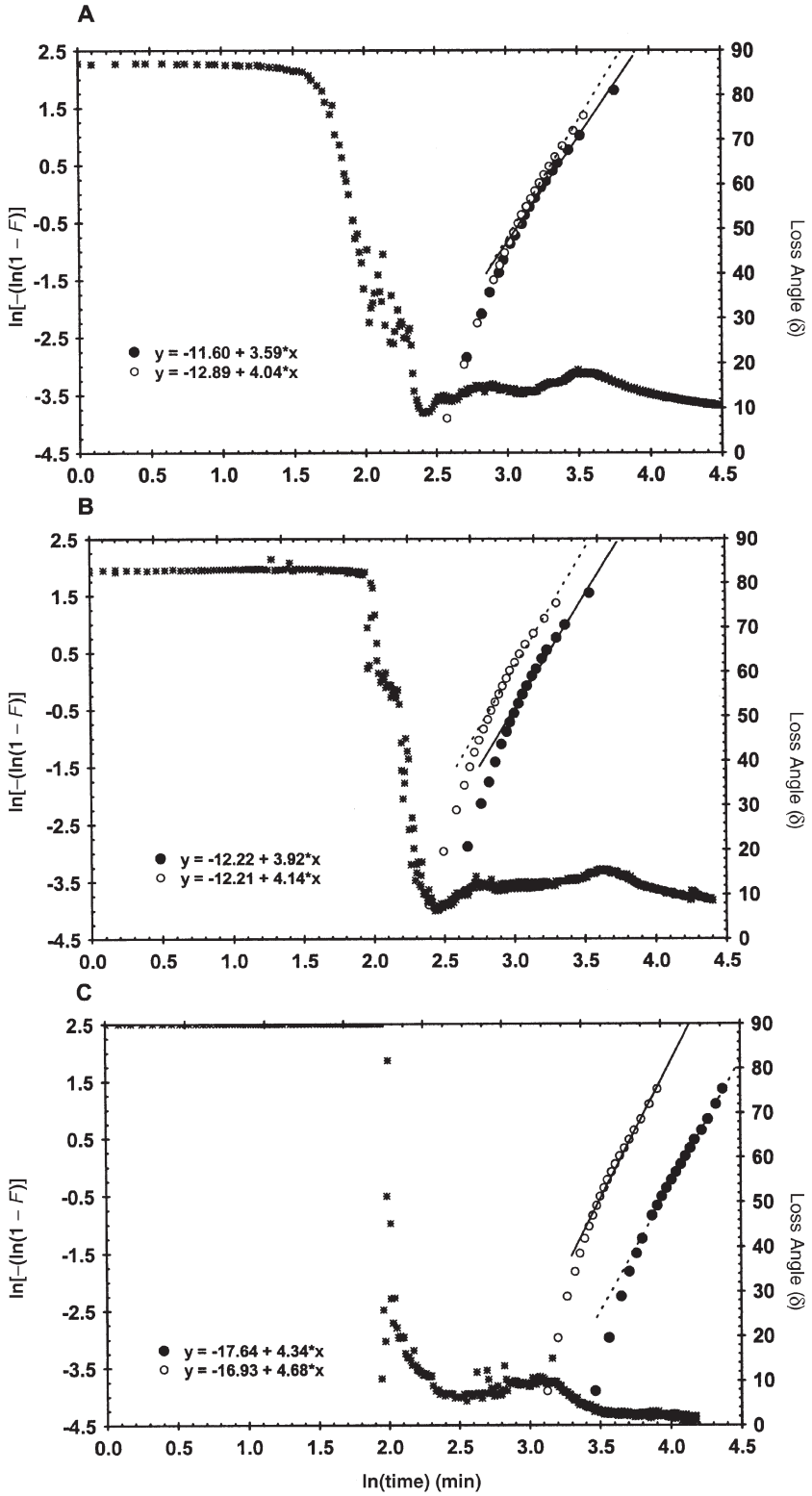

FIG. 5. Avrami plots for the 80% palm stearin/sesame oil blend at 36°C using a cooling rate of 1°C/min (A), 10°C/min (B), and 30°C/min (C). The rest of the legend is as in Figure 4.

of the local order of TAG molecules in the liquid state (i.e., lamellar structures), nucleation, and crystal growth. All these processes occurred during bulk crystallization of TAG in events occurring not sequentially but in parallel at different rates. Our results showed that the extent to which each of these processes was involved as a function of crystallization time depended on supercooling and the cooling rate. Thus, at low cooling rates (i.e., 1°C/min) and high degrees of

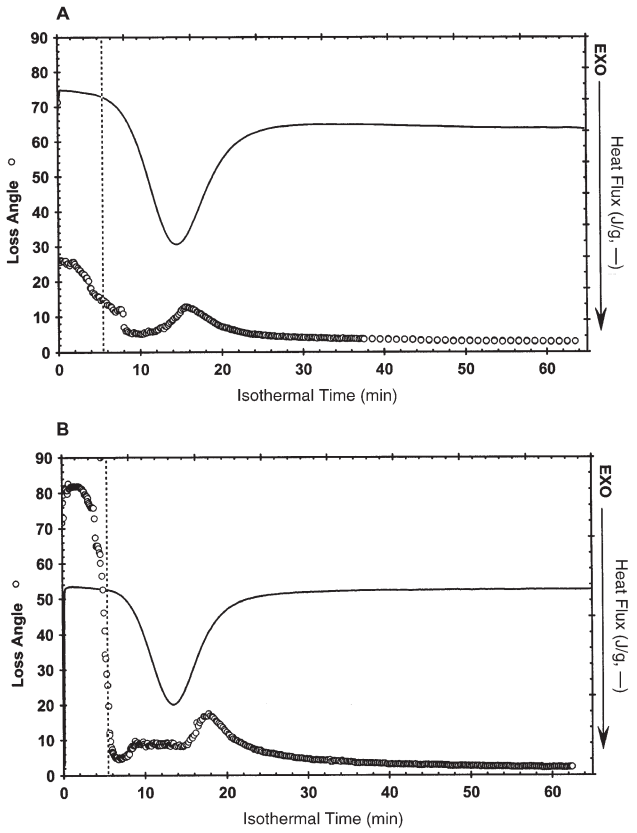

FIG. 6. Rheograms (loss angle, δ) and thermograms for the 80% palm stearin/sesame oil blend crystallized at 35°C at a cooling rate of 1°C/min (A) and 10°C/min (B). The vertical dotted line indicates the induction time of crystallization by DSC (τ_{iDSC}).

supercooling (i.e., low crystallization temperatures), TAG molecules developed local order in the liquid state (i.e., lamellar structures) while temperatures decreased toward isothermal conditions. In some cases, nucleation might even have occurred during the nonisothermal period (see Ref. 7). However, if the degree of supercooling was low enough (i.e., a high crystallization temperature) TAG molecules did not have enough time to develop the local order as temperatures decreased. Consequently, the local order of TAG molecules was developed during the isothermal period. A similar situation occurred at high cooling rates and high degrees of supercooling. Under such conditions TAG did not achieve the molecular order during cooling, and the local order for nucleation was attained during the isothermal period. The time involved during cooling before attainment of isothermal crystallization conditions was then calculated (Eq. 7) and its effect on the mechanism of crystal growth (n) evaluated. In Equation 7, T_M° is the equilibrium melting temperature for the oil blends (T_M° = 62.82°C, as established in Ref. 7), and T_{Cr}° is the temperature of crystallization to be achieved at a given cooling rate (°C/min). As previously mentioned, T_M° is the temperature at which the unstable crystal nuclei are in equilibrium with TAG in lamellar "liquid organization" in the vegetable oil. The use of this variable to analyze the crystallization process of the oil blends will be described shortly.

$$\text{time before attainment of isothermal conditions (min)} = (T_M^\circ - T_{Cr}^\circ)/(\text{°C/min}) \quad [7]$$

The conclusions discussed above showed that the sharp decrease in δ indicated the start of nucleation, whereas the δ peak indicated the predominance of the crystal growth process. Within this framework, it is postulated that the two slope regions observed in the Avrami plots were the result of a combined effect of the process of nucleation and crystal growth. Each event occurred at a different rate and extent as affected by cooling rate and T_{Cr}° (i.e., Eq. 7) and as a function of crystallization time under isothermal conditions at a given degree of supercooling. The shadow regions shown in Figure 4 are used to describe the relative contribution of nucleation and crystal growth to the entire process of crystallization. The proportion between the two areas was established based on the behavior of the δ profile and the crystallization exotherm. No actual calculations were done to establish the corresponding areas assigned to nucleation and crystal growth. The first region of the Avrami plot was mainly associated with nucleation, whereas the crystal growth process was mainly involved in the second region. Consequently, z, the complex rate constant involving nucleation and crystal growth rates, included the nucleation rate as its major component when calculated from the first region. In contrast, z for the second region had as its major component the crystal growth rate. By the same token, n, the value associated with the mechanisms of crystal growth, is better estimated from the second region of the Avrami plot. In fact, the statistical analysis showed that n calculated from the first region (data not shown) were, in all cases, above (i.e., $n > 4.0$, $P < 0.05$) the interval specified for the Avrami theory (9,10). In the same way, the linear regression between $F \geq 0.25$ and $F \geq 0.75$ also provided n values greater than 4 (data not shown). Such an F interval is commonly used (1) to calculate n and z, since this region of crystallinity ensures constant radial growth rate and no crystal impingement according to the Avrami crystal growth theory (9,10). In contrast, the n values calculated from the second region were within the interval specified for the Avrami equation (Table 1). The n values greater than 4 obtained at 35°C and a 10°C/min cooling rate and at 36°C at 10 and 30°C/min cooling rates (Table 1) were statistically not different from 4.0. This may indicate that under such crystallization conditions, the assumptions made by the Avrami model are difficult to accomplish (i.e., crystal impingement occurs at long crystallization times). Within this framework, further analysis of the crystal growth mechanism of TAG was done with n values calculated from the second region.

The effect of the time before attainment of isothermal conditions (Eq. 7) on n was evaluated for the different cooling rates investigated, independent of the concentration of PS in

TABLE 1
Values of *n* and *z* Determined from the Second Region of the Avrami Plot for Blends of Palm Stearin and Sesame Oil

	1°C /min[b]		10°C /min		30°C /min	
T_{Cr}[a]	*n*	$z \times 10^{-4}$	*n*	$z \times 10^{-4}$	*n*	$z \times 10^{-4}$
26%						
24.5	2.41 (0.39)[c]	27.8 (30.7)	3.20 (0.51)[c]	20.5 (25.9)	2.95 (0.06)[c]	1.63 (0.34)
25.5	3.05 (0.09)[d]	2.94 (1.01)	2.85 (0.19)[d]	1.24 (0.76)	3.84 (0.14)[d]	0.05 (0.02)
26.5	2.77 (0.21)[d]	4.40 (2.99)	3.57 (0.49)[d]	0.14 (0.17)	3.97 (0.07)[d]	0.01 (0.003)
27.5	3.23 (0.59)[d]	0.44 (0.32)	3.46 (0.13)[d]	0.07 (0.06)	3.35 (0.87)[c]	0.53 (0.74)
80%						
33.0	3.52 (0.31)[c]	3.03 (2.26)	3.51 (0.12)[c]	2.83 (0.07)	3.90 (0.75)[c]	2.17 (2.97)
34.0	3.87 (0.08)[c]	0.46 (0.10)	3.18 (0.52)[c]	6.75 (7.87)	3.98 (0.45)[c]	0.55 (0.71)
35.0	3.45 (0.26)[c]	0.77 (0.56)	4.10 (0.25)[d]	0.16 (0.13)	3.87 (0.31)[c]	0.17 (0.28)
36.0	3.82 (0.31)[c]	0.06 (0.05)	4.03 (0.16)[d]	0.04 (0.00)	4.51 (0.24)[d]	0.0003 (0)

[a]Crystallization temperature.
[b]Values in parentheses are SD of at least two replicates. For the same oil blend, different letters (c,d) in the same column indicate significant differences ($P < 0.01$).

the oil. The resulting plots are shown in Figure 7 along with the linear regressions obtained in each case. Overall, the linear regressions showed that, independent of the oil blend studied, as cooling time increased, the dimensionality of the crystal growth process decreased. In other words, for a given cooling rate, as the crystallization temperature decreased (i.e., supercooling increased) *n* also decreased. However, this effect was a function of the cooling rate used. Thus, the magnitude of the coefficient of determination (*r*) and its associated significance was higher at 1°C/min than at 10 or 30°C/min (Fig. 7). Consequently, at a cooling rate of 1°C/min the cooling time variable (Eq. 7) described ≈80% of the variance observed in *n* ($r^2 \cdot 100$). In contrast, only ≈46 and ≈49% of the magnitude of *n* was determined by this variable at 10 and 30°C/min. These results indicated that the cooling time before attainment of isothermal conditions is the main variable that determines the Avrami index at low cooling rates (i.e., 1°C/min). However, additional variables must be considered to better describe *n* at cooling rates of 10 and 30°C/min. Such variables might include heat and mass transfer conditions.

On the other hand, the *z* values for both the first (data not shown) and the second region (Table 1) decreased, in general, as temperature increased. This showed that the process of crystallization, including both nucleation and crystal growth processes, occurred at slower rates as temperature increased. However, according to the crystallization mechanism proposed in the present investigation, *z* from the first or the second region of the Avrami plot (Fig. 4) differed in proportion between the rates of nucleation and rates of crystal growth. Thus, *z* for the second region (Table 1) had as its major component the crystal growth rate, whereas for the first region the major component of *z* was nucleation rate. The higher variability observed by *z* in comparison to the one obtained with *n* resulted from the higher sensitivity of *z* to small changes in the slope (i.e., *n*). Such a situation occurred given the mathematical operation involved in the calculation of *z* [i.e., $e^{\ln(z)}$, Eq. 2].

The fractal dimension at the different cooling rates. Regarding the calculation of *D*, the experimental protocol followed by Narine and Marangoni (4) must be distinguished from the one used here. Narine and Marangoni used oil/fat systems (e.g., palm oil, cocoa butter, and tallow) crystallized under a dynamic regime, and the systems were then diluted with canola or soybean oil. The mass fractal dimension, *D*, was determined from the slope of the log–log relationship between the volume fraction of solid fat (ϕ) for each crystal dilution and the corresponding G'. In the present study, we measured G' as the oil blend crystallized under isothermal conditions. For the same crystallization time, the ln(G') was then associated with the corresponding ln(*F*). This last parameter was obtained from the corresponding DSC thermogram as described in the Materials and Methods section. As previously indicated, this approach assumed that $F \approx \phi$ (Eq. 6), which in turn implied that ϕ for all crystallization conditions investigated were normalized to *F* values between $0 \geq F \leq 1$. According to Equation 6, plots of ln(G') and ln(*F*) are shown in Figure 8. The different slopes (*m*) observed during the process of crystallization were associated with different stages of

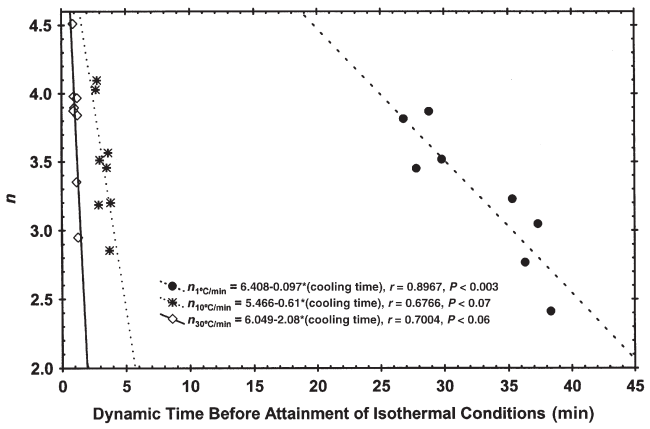

FIG. 7. Relationship between the Avrami index (*n*) and the time before attainment of isothermal conditions (i.e., cooling time) for the different cooling rates investigated.

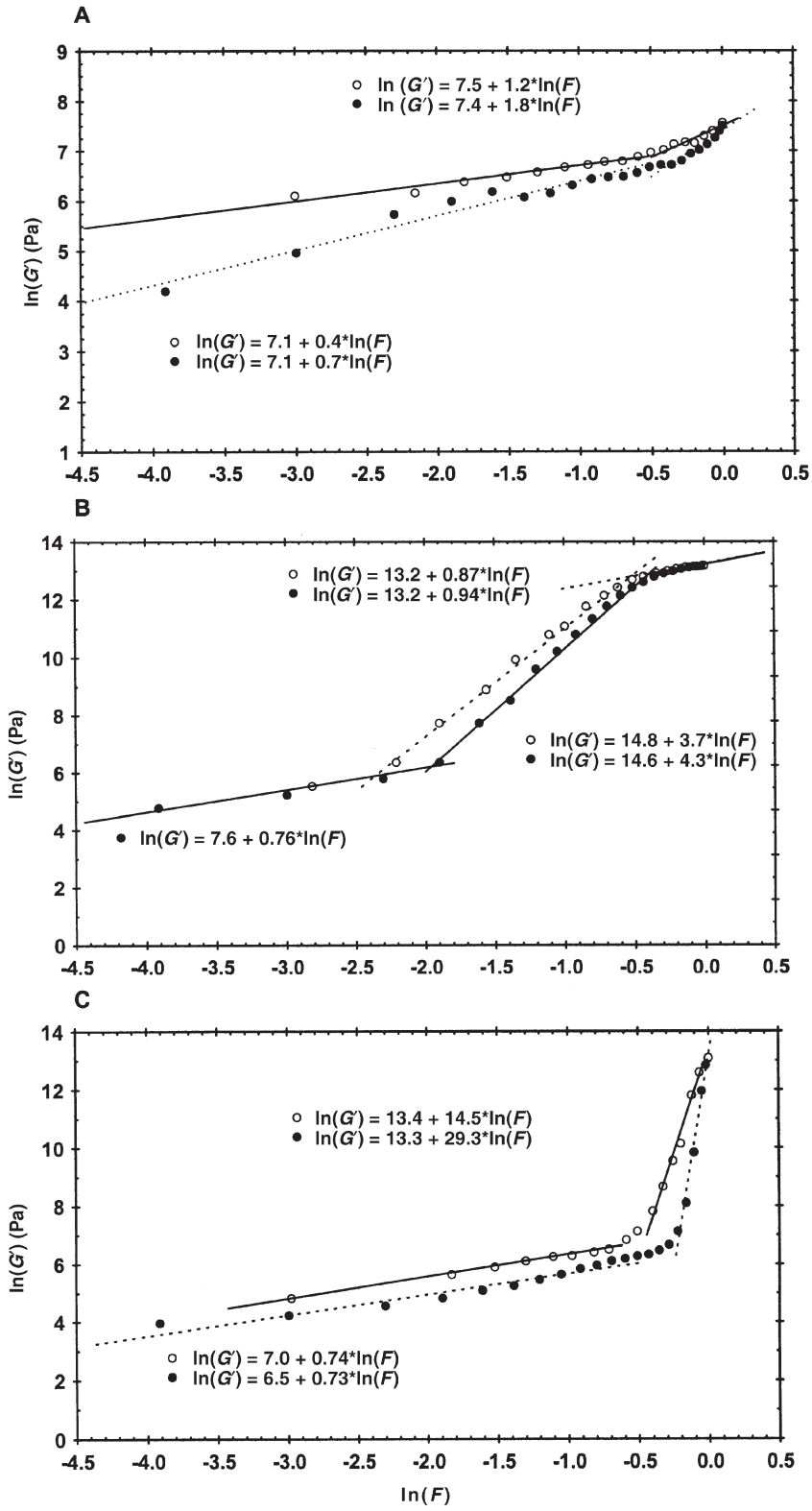

FIG. 8. Relationship between *G′* and *F* for the 26% oil blend crystallized at 24.5°C (A); for the 80% blends at 33°C (B) using a 1°C/min cooling rate; and for the 80% oil blends crystallized at 34°C using a 10°C/min cooling rate (C). Two replicates are shown.

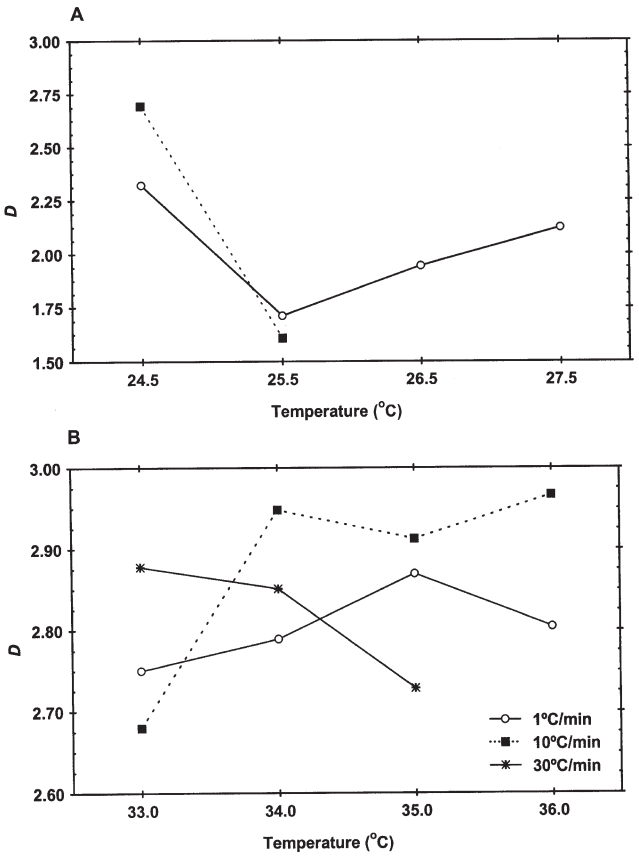

FIG. 9. Fractal dimension (*D*) for the 26 (A) and 80% (B) palm stearin/sesame oil blends as a function of the crystallization temperatures investigated.

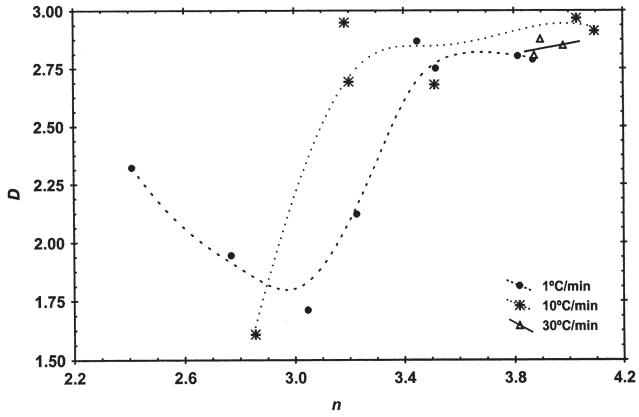

FIG. 10. Relationship between the Avrami index (*n*) and the fractal dimension (*D*) for the palm stearin/sesame oil blends at the different cooling rates investigated.

organization, gradually accomplished by the TAG crystals as a function of crystallization time. The first stage of the ln(G') vs. ln(F) plot provided m values lower than 1.0 in all cases. At this stage, a low volume fraction of TAG crystals was present. Consequently, no significant dimensionality of the TAG crystal network was achieved (i.e., D values lower than 1 were obtained). However, this stage was followed by the development of the actual fractal organization. Therefore, m values were obtained that, according to the weak-link regime, provided the dimensionality of the TAG crystal network (i.e., $1.0 \geq D \leq 3.0$). The fractal organization (D) attained under given crystallization conditions was then calculated from the slope corresponding to this stage using Equation 5 (Fig. 8). After this stage, a plateau followed, characterized by a slope that was not significantly different from zero ($m \approx 0$, $P < 0.05$). In some cases, this stage was evident right after the final fractal organization had been achieved (Fig. 8B). A high volume fraction of TAG crystals was present at this stage, but no significant linear relationship between ln (G') and ln(F) was observed. This indicated that no further change in the fractal dimension took place. The D values calculated accordingly had, in all cases, a variation coefficient lower than 13%.

A significant interaction between crystallization temperature and cooling rate affected the magnitude of D in both the 26 and the 80% ($P < 0.0001$) blends (Fig. 9). At low degrees of supercooling and high cooling rates, in both the 26 and 80% oil blends, the ln(G') vs. ln(F) plots provided slope values not different from zero ($P < 0.05$). This produced D values without physical meaning (i.e., negative D values). Such temperatures were 26.5 and 27.5°C for the 26% blend at 10°C/min, and 36°C for the 80% blend at 30°C/min. Under these crystallization conditions (i.e., low degrees of supercooling and high cooling rates), the development of a volume fraction of TAG crystals (ϕ) is low (4). In such cases, the strong-link regime might be applicable instead of the weak-link regime. The mathematical relationship for the determination of D under the strong-link regime is different, involving the determination of the backbone fractal dimension or tortuosity of the crystal network (x). Such values were not determined in the present research.

The statistical analysis of the D values (Fig. 9) showed that for the 26% blend, the lower crystallization temperature provided the larger D values at both 1°C/min (D = 2.32, SD = 0.19) and 10°C/min (D = 2.69, SD = 0.01) ($P < 0.005$) (Fig. 9A). At temperatures higher than 24.5°C, D decreased at both cooling rates, attaining a constant value of 1.85 (SD = 0.26)—this with the exceptions previously indicated for the D values corresponding to 26.5 and 27.5°C at 10°C/min. On the other hand, for the 80% blend (Fig. 9B) the largest D values were obtained at 10°C/min at $T_{Cr}° \geq 34$°C (D = 2.94, SD = 0.03), followed by D values obtained at 30°C/min at $T_{Cr}° \leq 34$°C (D = 2.87, SD = 0.09) ($P < 0.05$), and then the values at 1°C/min at $T_{Cr}° \geq 35$°C (D = 2.84, SD = 0.04) ($P < 0.02$). In contrast, the smallest D values were obtained at 1°C/min at crystallization temperatures ≤ 34°C (D = 2.77, SD = 0.03) and 10°C/min at 33°C (D = 2.68, SD = 0.02). Overall, for 1 and 10°C/min cooling rates with the 80% blend, D had a quadratic tendency to increase as crystallization temperature increased. However, the opposite occurred when 30°C/min was used, i.e., D decreased as crystallization temperature increased (≤34°C, D = 2.87, SD = 0.09; 35°C, D = 2.73, SD = 0.06). This last behavior

including the low development of TAG crystals at 36°C using 30°C/min cooling rate, which limited the calculation of *D* under the weak-link regime (Fig. 9B).

We concluded from the above observations that with the 26% oil blend at both cooling rates investigated, less compact (i.e., less dense, tenuous) crystal network structures were developed at $T_{Cr}° \geq 25.5$°C, since lower *D* values were obtained than at 24.5°C. With the 80% blend, denser crystal network structures were developed at 1°C/min at $T_{Cr}° \geq 35$°C and at 10°C/min at $T_{Cr}° \geq 34$°C than at lower crystallization temperatures. In contrast, at 30°C/min denser structures were obtained at $T_{Cr}° \leq 34$°C than at 35°C. Based on the results of Kawamura (11) and Toro-Vazquez *et al.* (7), the 26% oil blend at $T_{Cr}° \leq 25$°C crystallized as a mixture of α and β_1' crystals, whereas at temperatures of 26°C and above only the β_1 state was formed. In contrast, in the 80% blend TAG crystallized as the β_1' polymorph state at $T_{Cr}° \leq 34.5$°C, whereas at $T_{Cr}° \geq 35$°C they crystallized as the β_1 polymorph state (7,11). Hence, changes in *D* values were associated with different polymorphic states developed by the oil blends as a function of crystallization temperature. These results showed that the different polymorphic states developed by the system as a function of $T_{Cr}°$ affected the geometric organization of the TAG crystal network and therefore the behavior of *D*.

On the other hand, since the mechanism of the crystal growth process might have affected the geometric organization of the TAG crystal network, the relationship between *n* and *D* was evaluated at the cooling rates investigated. The resulting plot is shown in Figure 10. It is apparent that, independent of the concentration of PS-in-oil system used, *n* (i.e., the dimensionality of the crystal growth process) had a relationship with *D*. Overall, for the 1 and 10°C/min cooling rates, the increase in *n* from ≈3 (a disk-like crystal growth mechanism) to ≈ 4 (a spherulitic crystal growth mechanism) produced a curvilinear increase in *D* from ≈1.75 until a plateau was reached as *D* approached 3.0. In other words, the change from a disk-like to a spherulitic crystal growth mechanism increased the structural order of the TAG network. Then, besides the different polymorph states, the growth mechanism followed by TAG crystals (i.e., *n*) also affected the geometric organization of the TAG crystal network and subsequently the magnitude of *D*.

However, a different *n–D* relationship was found at $n < 2.7$ when the 1°C/min rate was used, and also at the cooling rate of 30°C/min. Narine and Marangoni (4) suggested that the geometric fractal organization of the TAG network mainly depends on heat and mass transfer. Within this framework, a particular oil blend (i.e., 26 or 80% PS oil blend) crystallized at the same temperature but using different cooling rates would have different heat and mass transfer conditions. Such conditions modify nucleation and subsequently the template for crystal growth and development of the TAG crystal network. It has been proposed that oils with instantaneous nucleation characteristics providing a high number of sites dissipate the heat of crystallization in a more efficient way, and subsequently the crystal network achieves a higher level of order (i.e., higher *D*) (4). Then the particular heat and/or mass transfer conditions existing under extreme crystallizing conditions (i.e., high degree of supercooling at the lowest cooling rate or a very high cooling rate) might be associated with the different behavior observed in the *n–D* relationship at $n < 2.7$ and at 30°C/min (Fig. 10).

The value of γ (i.e., pre-exponential term in Eq. 6) was calculated, and its relationship with *n* was evaluated for each of the oil blends used (data not shown). The parameter γ has been related to Young's modulus of individual particles that conform the network (12). Marangoni and Narine (13) have established the relationship between the elastic modulus (G') and the volume fraction of solid particles (in the present research, approximated by *F*). The same authors described the relationship between Young's modulus and the microstructure of particle aggregate networks. Thus, γ (Eq. 6) depends on the size of the particles within the floc, the interaction force between the flocs (i.e., force of the interfloc links), and the spatial distribution of solid particles within the network (11). In other words, γ is associated with the mechanical properties of the particles and the flocs that conform to the TAG crystal network. However, γ is independent of the volume fraction of solid particles (2). Our results showed that, independent of the cooling rate used, the 26% oil blend showed a maximum around $n \approx 3.0$ (i.e., 2-D growing mechanism) and the 80% oil blend at $n \approx 3.9$ (i.e., 3-D growing mechanism). This was independent of the cooling rate used. Such conditions correspond to temperatures of 25.5°C, for the 26% oil blend, and 34–35°C, for the 80% oil blend. Again, these crystallization conditions corresponded quite closely to polymorph changes occurring in the oil blends as a function of crystallization temperature. As previously indicated, the 26% oil blend crystallized as a mixture of α and β_1' crystals at $T_{Cr}° \leq 25$°C, whereas at 26°C temperatures and above, only the β_1' state was formed (7,11). In the 80% oil blend, TAG crystallized as β_1' at $T_{Cr}° \geq 34.5$°C and as the β_1 polymorph at $T_{Cr}° \geq 35$°C (7,11). However, γ for the 80% oil blend (i.e., 9.8 MPa at 34°C, 1°C/min) was between 100 and 1000 times larger than the corresponding values for the 26% oil blend (i.e., .007 MPa at 25°C, 1°C/min). Obviously, such differences in magnitude affect the final texture of the system, in spite of having similar *D* and/or *n* values.

The type of analysis described here might be carried out to evaluate the effect of crystallizing conditions, such as shear rate and supercooling, on the development of fractal structures in vegetable oils. In the same way, since γ is a constant dependent on the size of the primary particles and on the interactions between them (i.e., on the polymorphic nature of the TAG crystals), the $\ln(G')$ vs. $\ln(F)$ plots are potential tools to establish the relationship among the Avrami index, the polymorphic state, and the texture of the system as affected by the crystallizing conditions. Future research must involve the use of different types of vegetable oils, fats, and oil blends to establish such relationships under a wide scope of TAG compositions.

ACKNOWLEDGMENT

The present research was supported by Consejo Nacional de Ciencia y Tecnología (CONACYT) through grant #485100-5-28251B.

REFERENCES

1. Toro-Vazquez, J.F., M. Briceño-Montelongo, E. Dibildox-Alvarado, M.A. Charó-Alonso, and J. Reyes-Hernández, Crystallization Kinetics of Palm Stearin in Blends with Sesame Seed Oil, *J. Am. Oil Chem. Soc. 77*:297–310 (2000).
2. Marangoni, A.G., and D. Rousseau, Plastic Fat Rheology Is Governed by the Fractal Nature of the Fat Crystal Network and by Crystal Habit, in *Physical Properties of Fats, Oils, and Emulsifiers*, edited by N. Widlak, AOCS Press, Champaign, 1999, pp. 96–111.
3. Toro-Vazquez, J.F., E. Dibildox-Alvarado, V. Herrera-Coronado, and M.A. Charó-Alonso, Triacylglyceride Crystallization in Vegetable Oils: Application of Models, Measurements, and Limitations, in *Crystallization and Solidification Properties of Lipids*, edited by N. Widlak, R. Hartel, and S.S. Narine, AOCS Press, Champaign, 2001, pp. 53–78.
4. Narine, S.S., and A.G. Marangoni, Fractal Nature of Fat Crystal Networks, *Phys. Rev. E 59*:1908–1920 (1999).
5. Toro-Vazquez, J.F., and J.A. Gallegos-Infante, Viscosity and Its Relationship to Crystallization in a Binary System of Saturated Triacylglycerides and Sesame Seed Oil, *J. Am. Oil Chem. Soc. 73*:1237–1246 (1996).
6. Che Man, Y.B., T. Haryati, H.M. Ghazali, and B.A. Asbi, Composition and Thermal Profile of Crude Palm Oil and Its Products, *Ibid. 76*:237–242 (1999).
7. Toro-Vazquez, J.F., V. Herrera-Coronado, E. Dibildox-Alvarado, M.A. Charó-Alonso, and C.A. Gómez-Aldapa, Induction Time of Crystallization in Vegetable Oils. Comparative Measurements by Differential Scanning Calorimetry and Diffusive Light Scattering, *J. Food Sci. 67*:1057–1065 (2002).
8. Metin, S., and R.W. Hartel, Thermal Analysis of Isothermal Crystallization Kinetics in Blends of Cocoa Butter with Milk Fat or Milk Fat Fractions, *J. Am. Oil Chem. Soc. 75*:1617–1624 (1998).
9. Avrami, M., Kinetics of Phase Change. I. General Theory, *J. Chem. Phys. 7*:1103–1112 (1939).
10. Avrami, M., Kinetics of Phase Change. II. Transformation-Time Relations for Random Distribution of Nuclei, *Ibid. 8*:212–224 (1940).
11. Kawamura, K., The DSC Thermal Analysis of Crystallization Behavior in Palm Oil, *J. Am. Oil Chem. Soc. 56*:753–758 (1979).
12. Bremer, L.G.B., B.H. Bijsterbosch, R. Schrijvers, T. van Vliet, and P. Walstra, On the Fractal Nature of Structure of Casein Gels, *Colloids Surf. 51*:159–170 (1990).
13. Marangoni, A.G., and S.S. Narine, Elasticity of Fractal Aggregate Networks: Mechanical Arguments, in *Crystallization and Solidification Properties of Lipids*, edited by N. Widlak, R. Hartel, and S.S. Narine, AOCS Press, Champaign, 2001, pp. 153–159.

[Received May 28, 2002; accepted May 28, 2002]